Journal of Fluorine Chemistry 204 (2017) 98–106

Contents lists available at ScienceDirect

Journal of Fluorine Chemistry

journal homepage: www.elsevier.com/locate/fluor

Fluoride adsorption from aqueous solution using a protonated clinoptilolite and its modeling with artificial neural network-based equations

B.G. Saucedo-Delgado[a], D.A. De Haro-Del Rio[b], L.M. González-Rodríguez[a], H.E. Reynel-Ávila[c,d], D.I. Mendoza-Castillo[c,d], A. Bonilla-Petriciolet[d,*], J. Rivera de la Rosa[b]

[a] Instituto Politécnico Nacional, Unidad Profesional Interdisciplinaria de Ingeniería Campus Zacatecas, Zacatecas, 98160, Mexico
[b] Universidad Autónoma de Nuevo León, Nuevo León, 64451, Mexico
[c] CONACYT, Cátedras Jóvenes Investigadores, 03940, Mexico
[d] Instituto Tecnológico de Aguascalientes, Aguascalientes, 20256, Mexico

ARTICLE INFO

Keywords:
Fluoride adsorption
Clinoptilolite
Artificial neural network
Adsorption modeling
Zeolite protonation procedure

ABSTRACT

Water defluoridation properties of a protonated clinoptilolite has been studied and analyzed. This adsorbent has been obtained by a thermochemical treatment with NH_4Cl to protonate the zeolite surface and to increase its specific surface area. Results of adsorption kinetics and isotherms showed that the defluoridation properties of this protonated clinoptilolite were better than those reported for raw and modified zeolites with multivalent cations such as aluminum or iron. Defluoridation performance of this protonated clinoptilolite was endothermic and increased at acidic conditions in contrast to other zeolites modified with multivalent cations that should operate at pH ≥ 7 to maintain the adsorbent chemical stability. In addition, new models have been also developed to fit the fluoride adsorption on this protonated zeolite. These models were based on a hybridization of artificial neural networks and Langmuir and Pseudo-second order equations. Results showed that these hybrid models satisfactorily fitted the kinetics and isotherms of the fluoride adsorption on protonated clinoptilolite. These new models are promising to correlate and predict the fluoride adsorption with this zeolite or other types of adsorbents.

1. Introduction

Zeolites are crystalline aluminosilicates with interconnected microporosity that can be used as adsorbents for water pollution control including water defluoridation [1–4]. The most abundant natural zeolite on earth is clinoptilolite, which belongs to the heulandite family and is characterized by a ratio Si/Al > 4 [1]. Clinoptilolite is recognized as a low cost and a highly available adsorbent worldwide [1,5]. It has been widely used in the adsorption of cationic species in water treatment due to its negatively-charged framework that is counter-balanced by exchangeable cations such as K^+, Na^+, Mg^{2+} and Ca^{2+} [1,4,6]. However, this zeolite shows a poor affinity for anionic species in aqueous solutions including fluoride ions and, consequently, its adsorption capacities may be lower than 1 mg/g in water defluoridation [3,7,8]. This low anion affinity is the main disadvantage for the application of clinoptilolite and other zeolites as low cost adsorbents for facing water pollution caused by fluorides.

Surface properties of zeolites can be tailored for the removal of a specific water pollutant using a variety of chemical reagents [1,7,9]. Surfactants, metallic species and rare earths can be used to enhance the physicochemical characteristics of zeolites for the adsorption of anionic species such as uraniate, arsenate, nitrates and phosphates [7,10–12]. For the case of fluoride ions, multivalent cations such as Al^{3+}, Fe^{3+} and La^{3+} can be utilized to increase the removal efficacy of zeolites [3,8]. For example, stilbite was modified with $FeCl_3$ solutions to increase its fluoride adsorption properties where a maximum uptake of 2.36 mg/g was obtained at room temperature and pH ~ 7 [13]. Surface chemistry of hematite has been also tailored with Al^{3+} and La^{3+} ions to improve its fluoride removal where the maximum adsorption capacity was 0.56 mg/g [14]. In a recent study, Velazquez-Peña et al. [8] have reported the modification of clinoptilolite, mordenite and chabazite with iron and zirconium to enhance their defluoridation properties obtaining adsorption capacities up to 3.5 mg/g at pH 6–7 and 30 °C. Nevertheless, these surface treatment methods may have, as a main drawback, the high possibility of causing a secondary pollution due to the potential release of harmful compounds to the environment especially when the water defluoridation process operates at pH < 6.

A common approach applied to provide acid characteristics in

* Corresponding author.
E-mail address: petriciolet@hotmail.com (A. Bonilla-Petriciolet).

https://doi.org/10.1016/j.jfluchem.2017.11.002
Received 16 October 2017; Received in revised form 3 November 2017; Accepted 8 November 2017
Available online 08 November 2017

zeolite surfaces for catalytic applications is the use of ammonium ions with a subsequent thermal treatment to remove the ammonia and to anchor H^+ species [15,16]. This surface protonation may improve the zeolite interactions with anionic species. Although this strategy has been utilized to modify the physicochemical properties of zeolites in catalytic processes [17,18], there is a lack of adsorption applications with protonated zeolites including the removal of toxic anions such as fluoride ions in aqueous solution [3].

On the other hand, the modeling of the adsorption of water pollutants on zeolites is fundamental for process design and scale up [4]. The thermodynamic understanding of zeolite performance for fluoride adsorption could be difficult due to the complex adsorbent composition and the nonlinear relationships between the defluoridation capacity and the process operating parameters. Therefore, the mathematical representation of the fluoride-zeolite interactions is challenging and traditional adsorption models may fail in the fitting of both kinetic and equilibrium data.

Based on these facts, the aims of this study were to introduce a straightforward treatment method to tailor the surface properties of clinoptilolite for fluoride removal and to develop new adsorption models for a robust fitting of defluoridation kinetic and equilibrium data of this zeolite. Specifically, an effective method that improved the clinoptilolite surface chemistry for fluoride adsorption is described in this paper. This modification procedure was based on the use of an ammonium solution followed by a thermal treatment to protonate the zeolite surface and to increase its specific surface area. Kinetic and equilibrium studies were carried out for water defluoridation with this protonated clinoptilolite and its adsorption properties were analyzed and compared with other zeolites reported in literature. New models have been also developed to fit the fluoride adsorption data obtained with this adsorbent, which were based on a hybridization of artificial neural networks and Langmuir and Pseudo-second order equations. In summary, this paper contributes to insights on fluoride removal from aqueous solution with clinoptilolite and its modeling with novel adsorption equations.

2. Methodology

2.1. Preparation of a protonated clinoptilolite for fluoride adsorption and its physicochemical characterization

Natural clinoptilolite was obtained from a Mexican mine and this adsorbent had the next chemical composition: 64.4% SiO_2, 12.2% Al_2O_3, 1.13% Fe_2O_3, 0.54% Na_2O, 3.07% K_2O, 2.6% CaO and 0.5% MgO. Raw zeolite was sieved and treated with a solution of NaCl to homogenize the exchangeable ions. Specifically, 50 g of raw zeolite were mixed with 500 mL of 2 M NaCl solution and the suspension was stirred at room temperature and 500 rpm for 24 h. Zeolite was washed with distilled water and dried at 105 °C where this adsorbent was labeled as ZNA. In a second stage, zeolite ZNA was treated with ammonium chloride to provide positive sites and to promote anionic selectivity. The protonation of this zeolite was performed according to a procedure adapted from Ghasemian et al. [18]. Specifically, 12.5 g of ZNA were dispersed in 250 mL of NH_4Cl 1 M at room temperature for 24 h. This modified zeolite was washed with hot distilled water and dried at 105 °C and thermally treated at 500 °C for 3 h using a heating rate of 5 °C/min. Preliminary tests were performed and results showed that these conditions were the best for the protonation of clinoptilolite surface. This modified zeolite was labelled as ZAM1. Finally, both ZNA and ZAM1 were washed with deionized water, until obtaining a constant pH in the washing solution, dried and stored for their further usage in fluoride adsorption.

A physicochemical characterization of zeolites ZNA and ZAM1 was carried out. Textural parameters were determined using N_2 adsorption-desorption isotherms obtained with a Microactive for TriStar II Plus 2.03 device. Specific surface areas of zeolites were estimated with the Brunauer-Emmet-Teller method (BET), while the average pore diameter was obtained from the Barrett–Joyner–Halenda (BJH) model. The point of zero charge (p.z.c.) of both ZNA and ZAM1 was quantified using the methodology reported by Gatabi et al. [19]. X-ray diffraction was used to identify the crystalline phases of tested zeolites. This analysis was carried out with a PANalytical Empyrean X-ray diffractometer coupled to a copper-anode X-ray tube, and a PIXcel 1D detector. The CuKα radiation was nickel filtered and conducted at 45 kV and 40 mA using the Bragg-Brentano geometry. Zeolite samples were scanned within the 2θ angular range of 5 to 70° with a step size of 0.02626°. Diffraction results were processed with the software HighScore Plus and the structural database PDF2. FTIR analysis was also employed to characterize the surface chemistry of zeolites. A Thermo Scientific Nicolet iS10 FTIR spectrometer was used where zeolites samples were previously mixed with KBr to be analyzed as pellets. FTIR spectra were recorded using 32 scans and a resolution of 4 cm^{-1}.

2.2. Water defluoridation studies with clinoptilolite

Fluoride adsorption experiments were carried out with both zeolites ZNA and ZAM1, using a mean particle size of ~ 53 μm, and initial pollutant concentrations from 10 to 210 mg/L. All fluoride solutions were prepared with NaF (Sigma Aldrich) and deionized water. Kinetic and equilibrium studies were performed at batch reactors with different conditions of pH (i.e., 6 and 7) and temperature (i.e., 30 and 40 °C) employing an adsorbent ratio of 2 g/L. Preliminary trials indicated that the adsorption equilibrium was reached at 24 h under constant stirring of 120 rpm. Results of fluoride removal tests were used to calculated adsorption rates, thermodynamic parameters and maximum adsorption capacities for tested zeolites. All experiments were done by duplicate and average values were employed in data analysis. Fluoride adsorption capacities (q, mg/g) of zeolites were calculated with the mass balance equation

$$q = \frac{(C_0 - C)V}{m} \tag{1}$$

where C_0 (mg/L) is the initial fluoride concentration, C (mg/L) is the fluoride concentration after adsorption at time t (h), V (L) is the solution volume and m (g) is the zeolite mass. Zeolites were separated by centrifugation after fluoride adsorption and the pollutant concentration was quantified in the solution. Fluoride concentrations in all adsorption experiments were measured using an ion selective electrode with TISAB® reagent.

Fluoride adsorption enthalpies (ΔH^0, kJ/mol) were calculated from the isotherms obtained at pH 6 with the next equations

$$\Delta H^0 = R\frac{T_2 T_1}{T_2 - T_1}\ln\left(\frac{K_{T_2}}{K_{T_1}}\right) \tag{2}$$

$$K_T = \frac{C_A}{C_e} \tag{3}$$

where K_T is the equilibrium constant for fluoride adsorption at temperature T (K), C_A is the concentration of fluoride ions adsorbed onto the adsorbent at equilibrium (mg/L), C_e is the fluoride equilibrium concentration in the solution (mg/L) and R is the universal gas constant (kJ/mol K).

2.3. Models used for the correlation of fluoride adsorption on clinoptilolite

Fluoride adsorption data of clinoptilolite were modeled with kinetic and isotherm adsorption equations widely used for zeolites [4]. Pseudo first [20] and pseudo second order [21] equations were utilized for data fitting of fluoride adsorption kinetics. These two models assume a reaction-controlled process and are defined as

$$q_{t,PFO} = q_{te,PFO}(1 - \exp(-k_1 t)) \tag{4}$$

$$q_{t,PSO} = \frac{q_{te,PSO}^2 k_2}{1 + q_{te,PSO} k_2 t} \quad (5)$$

where $q_{t,PFO}$ and $q_{t,PSO}$ are the fluoride adsorption capacities estimated by the kinetic models in mg/g, k_1 is the pseudo first order rate constant in h^{-1} and k_2 is the pseudo second order rate constant in g/mg h.

Weber − Morris approach [22] was applied for the intraparticle diffusion analysis of fluoride adsorption kinetics

$$q_t = k_{id} t^{0.5} + B \quad (6)$$

where k_{id} is the intraparticle diffusion rate constant in mg/g $h^{0.5}$ and B in mg/g is a parameter related to the boundary layer thickness [23].

Langmuir [24] and Freundlich [25] equations were selected to correlate the fluoride adsorption isotherms of clinoptilolite

$$q_{e,L} = \frac{q_{m,L} K_L C_e}{1 + K_L C_e} \quad (7)$$

$$q_{e,F} = k_n C_e^{1/nF} \quad (8)$$

where $q_{m,L}$ is the monolayer adsorption capacity in mg/g, K_L is the Langmuir constant in L/mg, k_n ($mg^{1-1/nF}$ $L^{1/nF}$ g^{-1}) and nF are the adjustable parameters of Freundlich isotherm, respectively.

Parameters of adsorption equations were fitted with a non-linear regression procedure where the stochastic optimization method Simulated Annealing [26] was used for minimizing the next error function

$$F_{obj} = \sum_{i=1}^{ndat} \left(\frac{q_{i,calc} - q_{i,\exp}}{q_{i,\exp}} \right)^2 \quad (9)$$

where $q_{i,exp}$ is the experimental adsorption capacity, $q_{i,calc}$ is the adsorption capacity calculated with the model under analysis and *ndat* is the number of experimental points used in adsorption data correlation.

Alternatively, a hybrid approach for the modeling of fluoride adsorption kinetics and isotherms has been proposed in this study. This hybrid model was obtained from the integration of Langmuir and Pseudo-second order equations with a feedforward artificial neural network (ANNs). For interested readers, Ghaedi and Vafaei [27] have provided a review of ANNs modeling in the context of adsorption for water treatment. In particular, ANNs was used to determine the parameters of Langmuir and Pseudo-second order equations and the fluoride adsorption capacities were calculated with these parameters and the corresponding adsorption model. Since the adsorption efficacy of a zeolite depends on several operating parameters at batch reactors [4], this hybrid adsorption model included the process conditions (e.g., pH, temperature and initial concentration) used in fluoride adsorption experiments as independent variables. Then, the hybrid ANNs-Pseudo second order model was defined as

$$z_{1j} = \sum_{k=1}^{c} w_{1jk} z_k + w_{1jc+1} \frac{T}{T_{\max}} + \theta_{1j} \quad j = 1,..., n_{neul1} \quad (10)$$

$$y_{1j} = \frac{1}{(1 + \exp^{-z_{1j}})} \quad j = 1,..., n_{neul1} \quad (11)$$

$$z_{2j} = \sum_{k=1}^{n_{neul1}} y_{1k} w_{2jk} + \theta_{2j} \quad j = 1, 2 \quad (12)$$

$$k_{2,ANNs} = y_{21} = z_{21} \quad (13)$$

$$q_{te,ANNs} = y_{22} = z_{22} \quad (14)$$

$$q_{t,ANNs} = \frac{q_{te,ANNs}^2 k_{2,ANNs}}{1 + q_{te,ANNs} k_{2,ANNs} t} \quad (15)$$

On the other hand, the fluoride adsorption isotherms were calculated with the next ANNs-Langmuir model

$$z_{1j} = w_{1j1} \frac{C_e}{C_{e,\max}} + w_{1j2} \frac{pH}{pH_{\max}} + w_{1j3} \frac{T}{T_{\max}} + \theta_{1j} \quad j = 1,..., n_{neul1} \quad (16)$$

$$y_{1j} = \frac{1}{(1 + \exp^{-z_{1j}})} \quad j = 1,..., n_{neul1} = \quad (17)$$

$$z_{2j} = \sum_{k=1}^{n_{neul1}} y_{1k} w_{2jk} + \theta_{2j} \quad j = 1, 2 \quad (18)$$

$$K_{L,ANNs} = y_{21} = z_{21} \quad (19)$$

$$q_{m,ANNs} = y_{22} = z_{22} \quad (20)$$

$$q_{e,ANNs} = \frac{q_{m,ANNs} K_{L,ANNs} C_e}{1 + K_{L,ANNs} C_e} \quad (21)$$

where w_{ijk} and θ_{ij} are the weights and biases of the artificial neural network, respectively.

For adsorption kinetics and isotherms, it was assumed a feedforward artificial neural network with one hidden layer where n_{neul1} is the number of hidden neurons. These hybrid models are illustrated in Fig. 1. The same stochastic optimization method was used to train these hybrid ANNs models where the values of w_{ijk} and θ_{ij} were determined via the minimization of the error function given by Eq. (9). In this case, all adsorption data obtained at different operating conditions were employed for the modeling with this hybrid approach, which included 27 experimental points from isotherms and 72 from kinetics for each zeolite where 70% was utilized for ANNs training and 30% for testing and validation. Herein, it is convenient to remark that the hybrid ANNs models simultaneously fitted all adsorption data for each zeolite, while individual correlations of kinetics or isotherms were done with the traditional adsorption equations. The performance of the hybrid ANNs models with different hidden neurons (n_{neul1}) was compared with that obtained for traditional kinetic and isotherm equations.

3. Results and discussion

3.1. Fluoride adsorption on clinoptilolite

Fluoride adsorption kinetics are given in Fig. 2 for selected operating conditions and both zeolites. Kinetics showed that fluoride adsorption was fast where more than 80% of dissolved anions was removed at 2 h of operating time. This result suggested that water defluoridation was mainly performed in the external surface of both zeolites. Fluoride uptakes increased with a temperature increment at pH 6, see Fig. 2. Calculated adsorption rates k_1 and k_2 were 1.12–1.96 h^{-1} and 0.34–0.96 g/mg h for ZNA and 1.44–2.21 h^{-1} and 0.15–0.5 g/mg h for ZAM1, respectively. Overall, the fluoride adsorption rates of protonated clinoptilolite were higher than those obtained for zeolite ZNA. Note that larger values of k_2 indicated a lower fluoride adsorption rate.

Intraparticle diffusion analysis of fluoride adsorption on ZNA and ZAM1 is reported in Fig. 3 and Table 1. Plots of q_t versus $t^{0.5}$ showed a multilinearity behavior for the fluoride uptake with both zeolites at different operating conditions suggesting that several mechanisms may control this removal process [23]. In particular, this analysis also pointed out that the adsorption in the adsorbent external surface could play a relevant role in the removal of this water pollutant with clinoptilolite. Fluoride intraparticle diffusion rates k_{id} ranged from 0.17 to 0.59 mg/g $h^{0.5}$ for ZNA and from 0.36 to 1.55 mg/g $h^{0.5}$ for ZAM1, respectively. Diffusion rates were greater in ZAM1 due to the zeolite protonation increased the adsorbent porosity [18], see results of Table 2, thus reducing the diffusional resistance of fluoride ions. Values of parameter B for ZAM1 were higher than obtained for ZNA indicating a more significant impact of boundary layer effect on its fluoride removal [23].

Fluoride adsorption isotherms for the two zeolites are reported in Fig. 4. Defluoridation properties of protonated clinoptilolite ZAM1 were

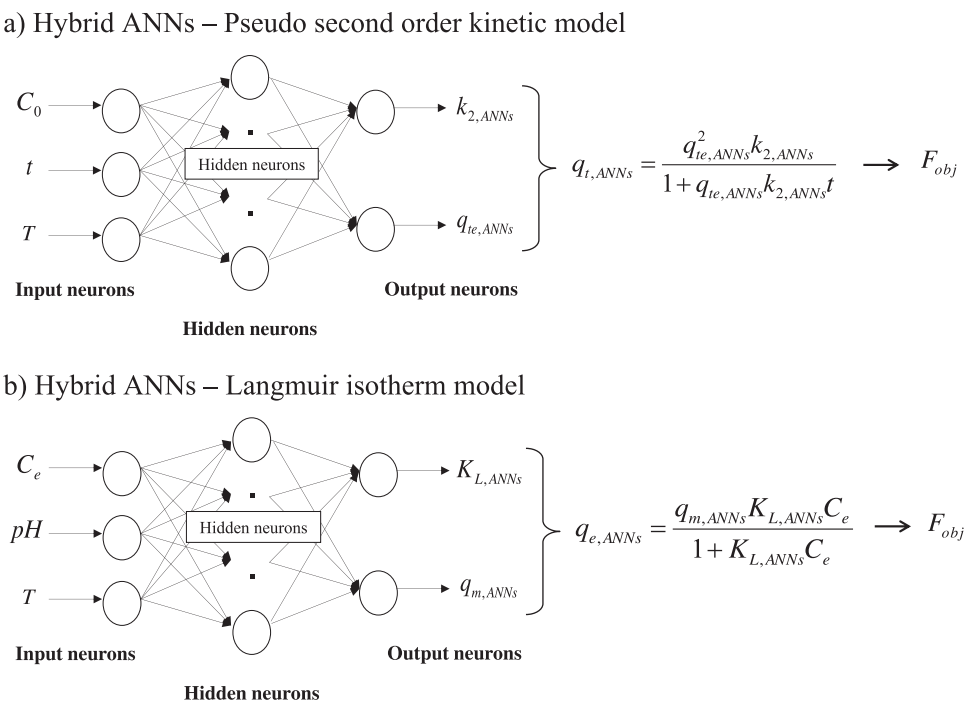

Fig. 1. Hybrid ANNs-adsorption models for the correlation of a) kinetics and b) isotherms of the fluoride removal with clinoptilolite.

better than those obtained for zeolite ZNA. The maximum fluoride adsorption capacities ranged from 1.5 to 5.3 mg/g for ZNA and from 6.3 to 12.4 mg/g for ZAM1 at tested operating conditions. Overall, these fluoride uptakes were higher than those reported for raw clinoptilolite (~2.5 mg/g) [6], mordenite (0.47 mg/g) [28] and other zeolites modified with iron, zirconium [8,13], aluminum, lanthanum [14] and calcium [29] where the adsorption capacities may range from 0.4 to 3.5 mg/g. These differences in defluoridation properties can be

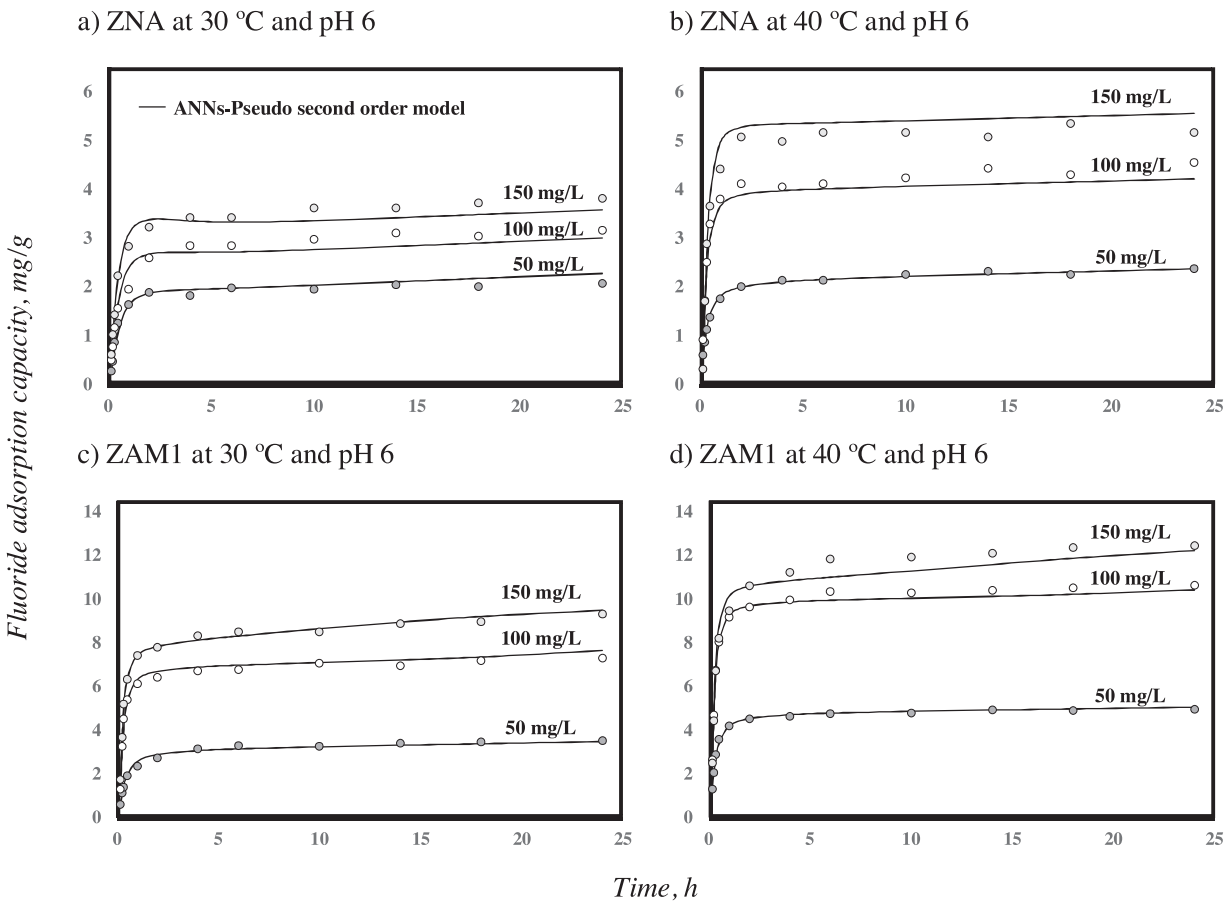

Fig. 2. Kinetics of fluoride adsorption on clinoptilolite at pH 6.

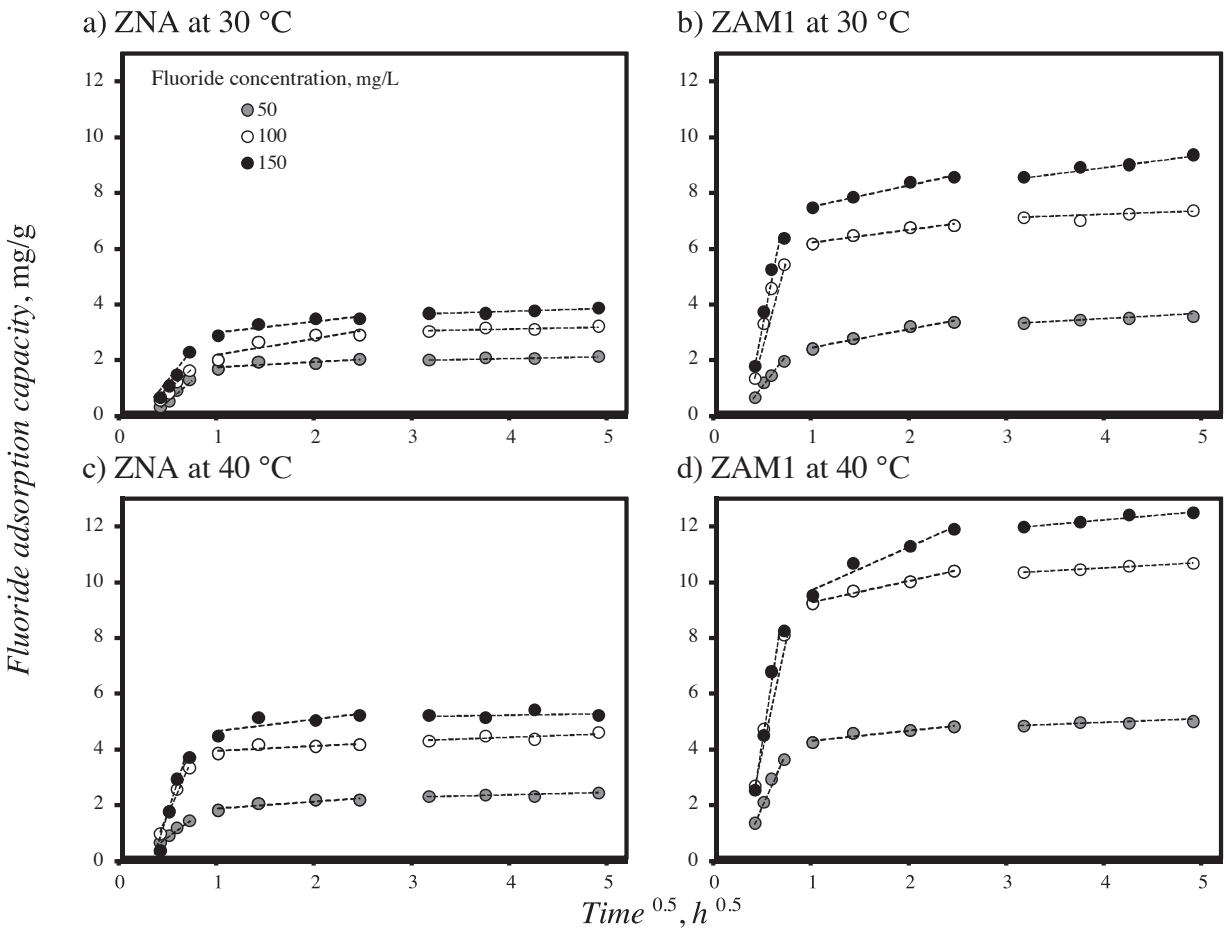

Fig. 3. Intraparticle diffusion analysis of fluoride adsorption on clinoptilolite at pH 6.

Table 1
Results of intraparticle diffusion analysis of the fluoride adsorption on clinoptilolite at pH 6.

			Intraparticle diffusion parameters		
Zeolite	C_0, mg/L	T, °C	k_{id}, mg/g $h^{0.5}$	B, mg/g	R^2
ZNA	50	30	0.19	1.50	0.68
		40	0.25	1.58	0.82
	100	30	0.59	1.55	0.79
		40	0.17	3.72	0.52
	150	30	0.40	2.54	0.82
		40	0.42	4.18	0.63
ZAM1	50	30	0.66	1.74	0.97
		40	0.36	3.90	0.90
	100	30	0.46	5.71	0.94
		40	0.77	8.45	0.99
	150	30	0.77	6.68	0.98
		40	1.55	8.12	0.95

Table 2
Textural properties of zeolites used in the fluoride adsorption from aqueous solution.

Zeolite	Surface Area S_{BET}, m^2/g	Pore Diameter, nm	Pore Volume, cm^3/g
ZNA	5.41	7.508	0.051
ZAM1	10.04	6.363	0.062

attributed to zeolite type, surface modification treatment and adsorbent size used in removal tests.

Results confirmed that both pH and temperature had a significant impact on the clinoptilolite removal performance. Specifically, a pH reduction from 7 to 6 caused an increment of 173 and 54% in the fluoride uptake of adsorbents ZNA and ZAM1, respectively. This pH-dependency was consistent with reported data for other zeolites used in fluoride adsorption [29]. This adsorption behavior can be attributed to the ionization of surface functional groups of zeolites and the reduction of the adsorption competition caused by OH^- ions due to pH changes [13,29]. However, it is important to highlight that zeolites modified with multivalent cations such as iron and zirconium may show a decrease of fluoride adsorption capacities when pH is reduced specially at acidic conditions [8,13]. This finding has been attributed to the leakage of active sites caused by the dissolution of the foreign cations introduced with the zeolite surface modification method [13]. Zeolites treated with multivalent cations should be used in water defluoridation at pH ≥ 7 to maintain the chemical stability of the adsorbent. Therefore, it is clear that the proposed approach to reverse the clinoptilolite surface charge was useful to improve its fluoride adsorption properties at acidic conditions and also offered additional advantages than those obtained with other zeolite surface modification protocols based on multivalent cations.

With respect to the thermodynamic nature of fluoride adsorption, the isotherms showed that this removal process was endothermic for both zeolites where the maximum adsorption capacities increased in ~ 28% with respect to a temperature raise from 30 to 40 °C at pH 6. Calculated fluoride adsorption enthalpies were 23.9 and 31.7 kJ/mol for ZNA and ZAM1, respectively. Other studies have reported the thermodynamic behavior of fluoride adsorption on different zeolites and results showed that it could be exothermic or endothermic depending on the adsorbent, e.g. [8,13]. For instance, clinoptilolite, mordenite and chabazite zeolites modified with iron and zirconium showed an exothermic adsorption behavior for fluoride removal at

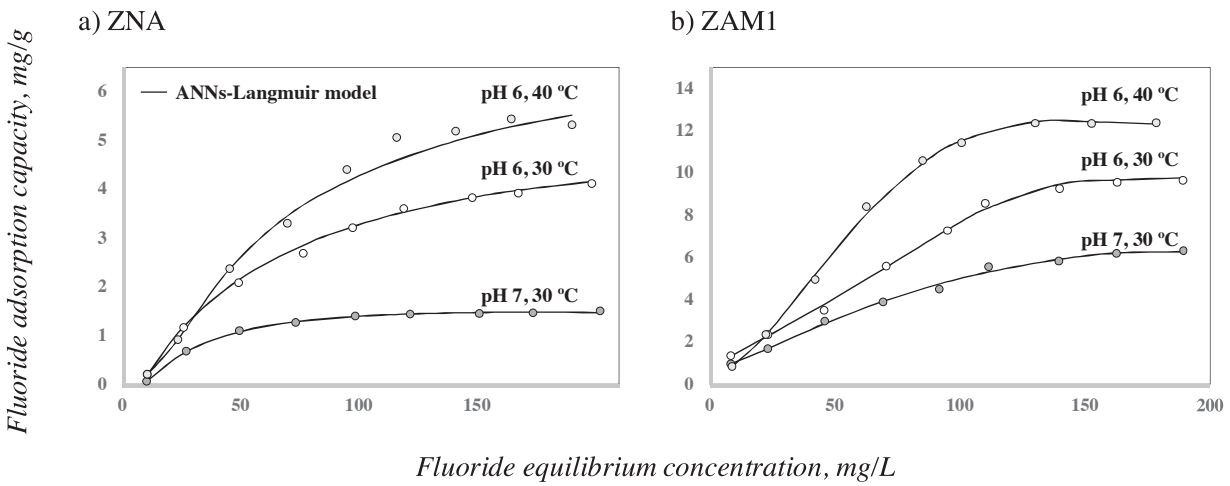

Fig. 4. Isotherms of fluoride adsorption on clinoptilolite.

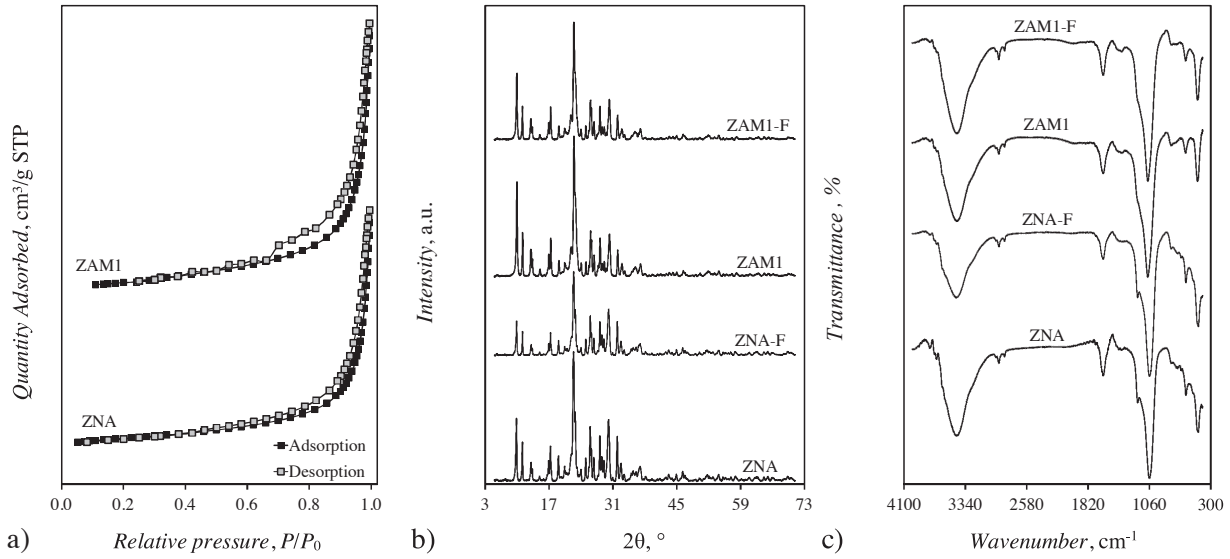

Fig. 5. Results of a) N_2 adsorption/desorption isotherms, b) X-ray diffraction and c) FTIR for zeolites used in fluoride adsorption.

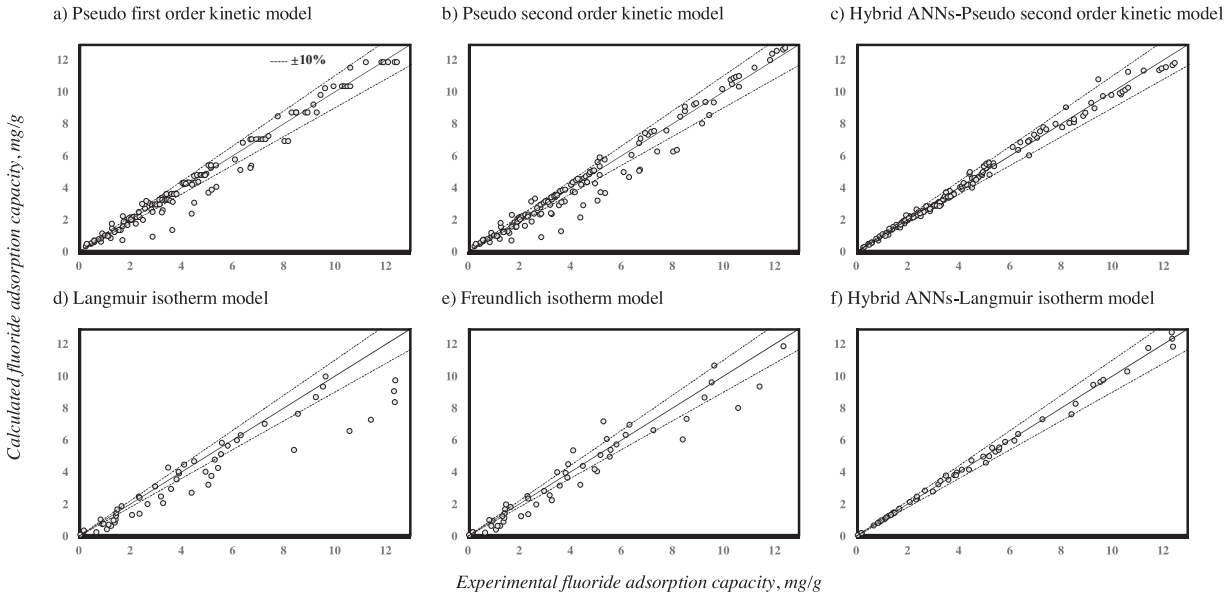

Fig. 6. Experimental and calculated adsorption capacities for the fluoride adsorption on clinoptilolite using kinetic and isotherm models.

Table 3
Kinetic parameters for the fluoride adsorption on clinoptilolite at different operating conditions.

			Pseudo first order model				Pseudo second order model			
Zeolite	C_0, mg/L	T, °C	$q_{te,PFO}$, mg/g	k_1, h^{-1}	R^2	e, %	$q_{te,PSO}$, mg/g	k_2, g/mg h	R^2	e, %
ZNA	50	30	2.02	1.12	0.93	11.12	2.26	0.49	0.86	14.45
		40	2.19	1.96	0.98	4.06	2.38	0.96	0.99	3.83
	100	30	2.97	1.23	0.99	6.04	3.32	0.39	0.98	6.88
		40	4.32	1.85	0.93	8.48	4.71	0.43	0.87	11.69
	150	30	3.61	1.33	0.97	6.52	4.02	0.34	0.94	9.09
		40	5.42	0.58	0.45	28.41	6.40	0.08	0.30	32.93
ZAM1	50	30	3.27	1.44	0.98	7.59	3.63	0.42	0.97	8.96
		40	4.80	2.19	0.97	4.76	5.18	0.50	0.94	7.35
	100	30	7.05	1.72	0.86	12.09	7.73	0.24	0.78	15.11
		40	10.36	2.21	0.95	6.41	11.17	0.23	0.89	9.59
	150	30	8.73	1.77	0.92	9.98	9.57	0.20	0.88	11.91
		40	11.87	1.75	0.95	7.70	13.03	0.15	0.93	8.99

Table 4
Results of data fitting for the fluoride adsorption kinetics on clinoptilolite using the hybrid ANNs − Pseudo second order model.

			Hidden neurons n_{neul1}					
			2		3		4	
Zeolite	C_0, mg/L	T, °C	R^2	e, %	R^2	e, %	R^2	e, %
ZNA	50	30	0.98	5.62	0.97	6.82	0.97	6.26
		40	0.98	11.12	0.99	1.97	0.99	1.77
	100	30	0.95	11.00	0.98	6.27	0.96	6.70
		40	0.97	16.90	0.99	4.65	0.99	5.24
	150	30	0.99	6.61	0.99	4.63	0.98	4.59
		40	0.97	12.53	0.99	6.71	0.99	6.68
ZAM1	50	30	0.98	4.87	0.97	5.73	0.99	3.42
		40	0.99	6.48	0.99	2.74	0.99	2.14
	100	30	0.98	4.84	0.98	6.31	0.99	4.53
		40	0.99	17.82	0.99	3.76	0.99	2.28
	150	30	0.98	12.01	0.99	3.47	0.99	1.63
		40	0.96	6.40	0.96	6.03	0.97	5.45

30–70 °C and pH 5.9 with enthalpy values from −18.15 to −4.58 KJ/mol [8]. In the contrary case, Zhang et al. [13] concluded that the fluoride removal using a natural zeolite modified with $CaCl_2$ was endothermic at pH 6 and 25–45 °C where the adsorption enthalpy ranged from 12.5 to 16.2 kJ/mol. Note that the fluoride adsorption enthalpies of several zeolites are typical of a physical adsorption [30]. Yao et al. [31] suggested that this result could be a consequence of the surface complexation variations that are taking place as adsorption temperature is modified.

Textural parameters and results of surface chemistry characterization of both zeolites are reported in Fig. 5 and Table 2. N_2 adsorption/desorption isotherms of these zeolites were typical of adsorbents with the presence of mesopores and a low external surface area [32]. A summary of textural properties of the adsorbents is presented in Table 2 where S_{BET} values were 5.41 m^2/g and 10.04 m^2/g for ZNA and ZAM1, respectively. There was a porosity increment of 90.6% caused by the zeolite protonation conditions, which could be related to a cation migration resulting into pore openings [33]. The average pore size of these zeolites was 7.508 and 6.363 nm, respectively, where ZAM1 showed a decrement of the average pore size but its pore volume increased in 22%, see Table 2. This change in surface properties can be mainly associated to the thermal treatment during clinoptilolite protonation [18,33]. On the other hand, the values of p.z.c. were 6.0 and 5.2 for ZNA and ZAM1, respectively, where the protonation procedure also decreased this surface parameter.

Table 6
Results of data fitting for the fluoride adsorption isotherms on clinoptilolite using the hybrid ANNs – Langmuir model.

			Hidden neurons n_{neul1}					
			2		3		4	
Zeolite	pH	T, °C	R^2	e, %	R^2	e, %	R^2	e, %
ZNA	7	30	0.98	5.19	0.99	1.16	0.99	1.79
	6	30	0.98	4.75	0.99	1.74	0.99	1.81
	6	40	0.99	4.15	0.99	3.40	0.99	2.32
ZAM1	7	30	0.98	4.57	0.99	2.80	0.99	2.02
	6	30	0.97	7.38	0.99	2.31	0.99	1.03
	6	40	0.98	5.74	0.99	3.23	0.99	1.62

X-ray diffraction results of ZNA and ZAM1 are given in Fig. 5b. Reflection patterns of these samples corresponded to the heulandite framework at 9.86°, 11.17° and 22.34° [34]. ZAM1 and ZNA exhibited practically the same X-ray reflection patterns. Results also indicated that the crystalline phases of the samples were clinoptilolite-Ca ($Na_{4.24}Ca_{1.80}K_{0.28}Mg_{0.16}Al_{8.16}Si_{27.84}O_{96.88}$) and coesite ($Si_{16.0}O_{32.0}$) being the first one the dominant phase (~90%). Also, the similar reflection intensity in both X-ray diffraction patterns of ZNA and ZAM1 indicated that the crystalline structure of the zeolite was not significantly modified after surface protonation. Similar findings have been reported by Ghasemian et al. [18] in the protonation of this type of zeolite for catalytic applications. After fluoride adsorption, a

Table 5
Parameters of Langmuir and Freundlich models for the fluoride adsorption on clinoptilolite at different operating conditions.

Zeolite	pH	T, °C	$q_{m,L}$, mg/g	K_L, L/mg	R^2	e, %	k_n, $mg^{1-1/nF}\ L^{1/nF}\ g^{-1}$	n_F	R^2	e, %
ZNA	6	30	19.99	1.46E-03	0.84	23.47	2.20E-02	0.96	0.74	24.67
		40	19.99	1.70E-03	0.61	34.11	1.70E-02	0.86	0.73	25.61
	7	30	19.99	4.50E-04	0.20	36.48	5.50E-03	0.90	0.40	34.93
ZAM1	6	30	17.32	7.20E-03	0.96	9.50	2.90E-01	1.45	0.97	8.22
		40	19.99	7.00E-03	0.76	25.99	1.30E-01	1.09	0.81	16.54
	7	30	9.44	1.08E-02	0.97	6.25	2.50E-01	1.57	0.99	5.35

Table 7
Parameters of hybrid ANNs adsorption models used for fitting the fluoride removal with clinoptilolite.

		Zeolite			
		ZNA		ZAM1	
Parameter	ijk	Kinetic model	Isotherm model	Kinetic model	Isotherm model
w_{ijk}	111	−10.00	2.10	−0.18	7.32
	112	−0.10	9.15	0.01	−1.61
	113	−0.19	−1.28	−2.64	0.60
	121	0.03	−0.08	0.02	4.38
	122	−1.25	−6.48	−3.88	−7.29
	123	4.13	6.24	1.11	5.34
	131	−0.03	−9.41	10.00	1.68
	132	−0.03	−0.27	0.02	0.22
	133	−1.43	0.48	1.02	−1.59
	211	−500.00	387.83	146.27	268.02
	212	87.99	−231.57	5.46	−448.50
	213	60.19	118.49	190.06	247.52
	221	−9.47	274.92	−476.63	−10.75
	222	−177.51	185.57	−93.56	17.10
	223	−151.00	−38.69	−25.40	90.10
θ_{ij}	11	−3.91	−2.71	−2.17	−5.06
	12	−7.17	5.44	−2.28	−0.90
	13	−1.26	−3.34	2.82	3.62
	21	2.11	−152.13	−187.48	23.07
	22	17.16	−453.72	41.07	−83.87

decreased in the reflection intensities was observed. This result could be attributed to changes in the sample crystallinity due to the adsorption of fluoride ions [14].

Results of FTIR characterization of both zeolites, before and after fluoride adsorption, are reported in Fig. 5c. For zeolite ZNA, the band at 1059 cm^{-1} and the shoulder at 1150 cm^{-1} can be associated to asymmetric stretching mode of T-O internal tetrahedron vibrations where T = Si or Al [8,35]. The band of O-T-O bending mode is identified at 453 cm^{-1} [8,35], while the other band at 780 cm^{-1} can be assigned to the T-O symmetric stretching vibration [8]. The bands observed at 780, 714 and 605 cm^{-1} correspond to double ring vibrations [8,36]. The bands at 3435 and 1631 cm^{-1} are associated to intermolecular hydrogen bonding and the bending mode of water, respectively [8]. According to Faghihian and Kabiri-Tadi [35], these water molecules can be linked with the exchangeable Na and Ca in the channels and cages of the zeolite structure. FTIR spectra of protonated zeolite showed the same major bands that were identified for ZNA. However, the bands at 3435 and 1631 cm^{-1} exhibited slight displacements and reductions that could be associated to the zeolite surface protonation [37]. The intensity and position of the bands related to the T-O and O-T-O also remained constant. This finding also indicated that the surface protonation did not affect the clinoptilolite skeleton structure [38]. After fluoride adsorption, ZNA showed slight displacements and reductions in the bands at 3435 and 1631 cm^{-1} that are related to the intermolecular hydrogen bonds of water thus suggesting their role in fluoride adsorption [8]. On the other hand, FTIR spectrum of ZAM1 did not show notable changes in the intensity or position of the aforementioned bands. According to these results, the zeolite surface was partially modified.

These characterization results suggested that fluoride adsorption using these zeolites could involve an ion exchange mechanism where fluorides might replace the hydroxyl ions of zeolite surface and there could be also the presence of van der Waals forces especially for the protonated zeolite ZAM1 causing that the positively charged surface of this zeolite might attract the fluoride ions [6,8].

3.2. Fluoride adsorption modeling with hybrid ANNs-based equations

Results of adsorption data modeling of both fluoride adsorption kinetics and isotherms are reported in Fig. 6 and Tables 3–6. Pseudo first and pseudo second order kinetic models showed modeling errors from 0.08 to 66.9% and from 0.001 and 68.0%, respectively. The determination coefficients R^2 of Pseudo first order model were higher than those obtained for the Pseudo second order kinetic equation. However, both models failed to fit the kinetic data of fluoride adsorption on ZNA at 150 mg/L and 40 °C where $R^2 < 0.5$, see Table 3. In general, the major deviations between predicted and experimental kinetic data of both models were observed at $q_t < 3$ where the errors could be higher than 60%. In contrast, the hybrid ANNs-Pseudo second order model showed the best fitting at all tested conditions with R^2 values ranging from 0.95 to 0.99 and modeling errors lower than 27.5%, see Fig. 6 and Table 4.

On the other hand, Freundlich model outperformed Langmuir equation in the correlation of fluoride adsorption isotherms on clinoptilolite, see results given in Table 5 and Fig. 6. But these two models showed low R^2 values and high modeling errors (i.e., up to 77%) for fitting the isotherms of ZNA especially at pH 7 and 30 °C. For tested zeolites, the modeling of isotherms was more challenging in comparison with kinetic data using the traditional adsorption equations. These results confirmed that the data modeling for this type of adsorbents may be complex and traditional adsorption equations may show a significant uncertainty. ANNs-Langmuir model offered the best performance to correlate the experimental isotherms at all conditions of pH and temperature. Modeling errors of this hybrid equation ranged from 0.001 to 9.2% with $R^2 \geq 0.98$, see results given in Table 6.

Hybrid ANNs adsorption models were tested with different numbers of hidden neurons (i.e., from 2 to 4) and results are reported in Tables 4 and 6. As expected, the increase of hidden neurons improved data correlation reducing significantly the modeling errors and allowed to obtain the best R^2 values. Note that the overfitting of these hybrid ANNs models was not identified at tested conditions. However, the models with three hidden neurons can provide the best performance in the correlation of the experimental data and, consequently, they are recommended to fit and predict the fluoride adsorption on clinoptilolite. Parameters of the best hybrid adsorption models are reported in Table 7.

In summary, these hybrid models showed a high curve-fitting capability for fluoride adsorption kinetic and isotherm data. This type of model offers the flexibility of reliably correlating the performance of clinoptilolite in fluoride adsorption at different operating conditions. The incorporation of an artificial neural network to determine the parameters of both Pseudo second order and Langmuir equations allowed obtaining a better fit in the fluoride adsorption modeling. Herein, it is convenient to remark that it was necessary to determine the parameters of traditional adsorption models, i.e., Eqs. (4)–(8), using a set of experimental data obtained at given operating conditions (e.g., fluoride initial concentration, pH and temperature). Therefore, these models are not useful for predicting the adsorption behavior of clinoptilolite at different operating conditions beyond the experimental range used in parameter estimation. However, hybrid ANNs adsorption equations used a single set of model parameters to fit simultaneously all experimental data and to predict with confidence the water defluoridation performance of tested zeolites at other operational scenarios.

4. Conclusions

This study has introduced a low-cost surface modification method to improve the water defluoridation properties of clinoptilolite and new adsorption equations for its modeling. The protonation of clinoptilolite was effective to increase its fluoride adsorption properties without altering significantly its crystalline structure but increasing its specific

surface area. This tailored clinoptilolite showed better fluoride adsorption capacities than those reported for other zeolites modified with multivalent cations. Maximum fluoride adsorption capacity of this protonated zeolite was 12.4 mg/g and defluoridation performance was endothermic and increased at acidic conditions in contrast to other modified zeolites that should operate at pH ≥ 7 to maintain the adsorbent chemical stability. Results showed that the hybridization of traditional adsorption equations with an artificial neural network was useful to develop new models to fit both kinetics and isotherms of the fluoride adsorption on protonated clinoptilolite. These new equations are promising to model and predict the fluoride adsorption with this zeolite or other type of adsorbents.

References

[1] S. Wang, Y. Peng, Natural zeolites as effective adsorbents in water and wastewater treatment, Chem. Eng. J. 156 (2010) 11–24.
[2] A. Bhatnagar, E. Kumar, M. Sillanpaa, Fluoride removal from water by adsorption −a review, Chem. Eng. J. 171 (2011) 811–840.
[3] P. Loganathan, S. Vigneswaran, J. Kandasamy, R. Naidu, Defluoridation of drinking water using adsorption processes, J. Hazard. Mater. 248-249 (2013) 1–19.
[4] M. Delkash, B.E. Bakhshayesh, H. Kazemian, Using zeolitic adsorbents to cleanup special wastewater streams: a review, Micropor. Mesopor. Mat. 214 (2015) 224–241.
[5] J. Behin, H. Kazemian, S. Rohani, Sonochemical synthesis of zeolite NaP from clinoptilolite, Ultrason. Sonochem. 28 (2015) 400–408.
[6] Q. Cai, B.D. Turner, D. Sheng, S. Sloan, The kinetics of fluoride sorption by zeolite: effects of cadmium: barium and manganese, J. Contam. Hydrol. 177-178 (2015) 136–147.
[7] H. Figueiredo, C. Quintelas, Tailored zeolites for the removal of metal oxyanions: overcoming intrinsic limitations of zeolites, J. Hazard. Mater. 274 (2014) 287–299.
[8] G.C. Velazquez-Peña, M.T. Olguín-Gutiérrez, M.J. Solache-Ríos, C. Fall, Significance of FeZr-modified natural zeolite networks on fluoride removal, J. Fluorine Chem. 202 (2017) 41–53.
[9] P. Misaelides, Application of natural zeolites in environmental remediation: a short review, Micropor. Mesopor. Mat. 144 (2011) 15–18.
[10] A.M. Yusof, N.A.N.N. Malek, Removal of Cr(VI) and As(V) from aqueous solutions by HDTMA-modified zeolite Y, J. Hazard. Mater. 162 (2009) 1019–1024.
[11] P. Chutia, S. Kato, T. Kojima, S. Satokawa, Adsorption of As(V) on surfactant-modified natural zeolites, J. Hazard. Mater. 162 (2009) 204–211.
[12] L.M. Camacho, R.R. Parra, S. Deng, Arsenic removal from groundwater by MnO_2-modified natural clinoptilolite zeolite: effects of pH and initial feed concentration, J. Hazard. Mater. 189 (2011) 286–293.
[13] Y. Sun, Q. Fang, J. Dong, X. Cheng, J. Xu, Removal of fluoride from drinking water by natural stilbite zeolite modified with Fe(III), Desalination 277 (2011) 121–127.
[14] A. Teutli-Sequeira, V. Martínez-Miranda, M. Solache-Ríos, I. Linares-Hernández, Aluminum and lanthanum effects in natural materials on the adsorption of fluoride ions, J. Fluorine Chem. 148 (2013) 6–13.
[15] E. Díaz, S. Ordóñez, A. Vega, J. Coca, Evaluation of different zeolites in their parent and protonated forms for the catalytic combustion of hexane and benzene, Micropor. Mesopor. Mat. 83 (2005) 292–300.
[16] Y. Kohno, Y. Shibata, N. Oyaizu, K. Yoda, M. Shibata, R. Matsushima, Stabilization of flavylium dye by incorporation into the pore of protonated zeolites, Micropor. Mesopor. Mat. 114 (2008) 373–379.
[17] N. Ghasemian, C. Falamaki, M. Kalbasi, M. Khosravi, Enhancement of the catalytic performance of H-clinoptilolite in propane-SCR-NOx process through controlled dealumination, Chem. Eng. J. 252 (2014) 112–119.
[18] N. Ghasemian, C. Falamaki, M. Kalbasi, Clinoptilolite zeolite as a potential catalyst for propane-SCR-NOx: performance investigation and kinetic analysis, Chem. Eng. J. 236 (2014) 464–470.
[19] M.P. Gatabi, H.M. Moghaddam, M. Ghorbani, Point of zero charge of maghemite decorated multiwalled carbon nanotubes fabricated by chemical precipitation method, J. Mol. Liq. 216 (2016) 117–125.
[20] S. Lagergren, About the theory of so-called adsorption of soluble substances, Kungliga Svenska Vetenskapsakademiens. Handlingar 24 (1898) 1–39.
[21] Y.S. Ho, G. McKay, The kinetics of sorption of divalent metal ions onto sphagnum moss peat, Water Res. 34 (2000) 735–742.
[22] W.J. Weber, J.C. Morris, Kinetics of adsorption on carbon from solution, J. Sanitary Eng. Div. 89 (1963) 31–60.
[23] K.L. Tan, B.H. Hameed, Insight into the adsorption kinetics models for the removal of contaminants from aqueous solutions, J. Taiwan Inst. Chem. Eng. 74 (2017) 25–48.
[24] I. Langmuir, The adsorption of gases on plane surface of glass mica and platinum, J. Am. Chem. Soc. 40 (1918) 1361–1403.
[25] H.M.F. Freundlich, Over the adsorption in solution, J. Phys. Chem. 57 (1906) 385–471.
[26] A. Bonilla-Petriciolet, M.G. Lira-Padilla, C. Soto-Becerra, Aplicación del método de optimización de recocido simulado en la regresión de isotermas de adsorción, Rev. Int. Cont. Amb. 21 (2005) 201–206.
[27] A.M. Ghaedi, A. Vafaei, Application of artificial neural networks for adsorption removal of dyes from aqueous solution: a review, Adv. Colloid Interfac. 245 (2017) 20–39.
[28] L. Gómez-Hortigüela, J. Pérez-Pariente, R. García, Y. Chebude, I. Díaz, Natural zeolites from ethiopia for elimination of fluoride from drinking water, Separ. Purif. Technol. 120 (2013) 224–229.
[29] Z. Zhang, Y. Tan, M. Zhong, Defluorination of wastewater by calcium chloride modified natural zeolite, Desalination 276 (2011) 246–252.
[30] Y. Liu, Y.J. Liu, Biosorption isotherms: kinetics and thermodynamics, Separ. Purif. Technol. 61 (2008) 229–242.
[31] W. Yao, X. Wang, Y. Liang, S. Yu, P. Gu, Y. Sun, C. Xu, J. Chen, T. Hayat, A. Alsaedi, X. Wang, Synthesis of novel flower-like layered double oxides/carbon dots nanocomposites for U(VI) and 241 Am(III) efficient removal: batch and EXAFS studies, Chem. Eng. J. 332 (2018) 775–786.
[32] M. Donohue, G. Aranovich, Classification of Gibbs adsorption isotherms, Adv. Colloid Interfac. 76–77 (1998) 137–152.
[33] D.B. Akkoca, M. Yılgın, M. Ural, H. Akçin, A. Mergen, Hydrothermal and thermal treatment of natural clinoptilolite zeolite from Bigadiç, Turkey: an experimental study, Geochem. Int. 51 (2013) 495–504.
[34] M.M.J. Treacy, Collection of simulated XRD powder patterns for zeolites, Appl. Catal. 21 (1986) 388–389.
[35] H. Faghihian, M. Kabiri-Tadi, Removal of zirconium from aqueous solution by modified clinoptilolite, J. Hazard. Mater. 178 (2010) 66–73.
[36] J. Li, J. Qiu, Y. Sun, Y. Long, Studies on natural STI zeolite: modification structure, adsorption and catalysis, Micropor. Mesopor. Mat. 37 (2000) 365–378.
[37] B. Muir, T. Badja, Organically modified zeolites in petroleum compounds spill cleanup −production efficiency, utilization, Fuel Process. Technol. 149 (2016) 153–162.
[38] H. Lin, Q. Liu, Y. Dong, Y. He, L. Wang, Physicochemical properties and mechanism study of clinoptilolite modified by NaOH, Micropor. Mesopor. Mat. 218 (2015) 174–179.